Retrieving Aerosols from the Atmospheric Emitted Radiance Interferometer: Can it be Done?

L. Moy, H.E. Revercomb, and R.O. Knuteson
Cooperative Institute for Meteorological Satellite Studies (CIMSS)
Madison, Wisconsin

D.D. Turner and E. Kassianov
Pacific Northwest National Laboratory
Richland, Washington

The Atmospheric Emitted Radiance Interferometer observes downwelling infrared radiance from 3-19 μm that may enable better retrievals of aerosol optical and physical properties. Theoretical study suggests that the Atmospheric Emitted Radiance Interferometer's infrared aerosol signal is strong enough to overcome instrument noise constraints and uncertainties in the water vapor, especially in the 3-4 μm band where scattering dominates the observed signal during the daytime. Unlike other aerosol retrieval methods that generally use wavelengths below 1 μm, the Atmospheric Emitted Radiance Interferometer's signal is dominated by the contribution from larger aerosols in the size distribution. We have retrieved aerosol optical depth for a range of assumptions of the number of giant particles in the size distribution; these retrievals together with aerosol optical depth retrieved from the multi-filter rotating shadowband radiometer can be used to determine the relative number of giant mode aerosols. Furthermore, different aerosol compositions have unique spectral signatures, which can be exploited in the retrievals.

Introduction

The scientific community's level of understanding about aerosols' radiative forcing of the climate system is "very low" (IPCC 2001). Accurate observations and theoretical knowledge of aerosols are needed, and new techniques are required in order to capture the large spatial and temporal variability of the aerosols and to provide sensitivity to the contributions from all particles in the size distribution.

The Atmospheric Emitted Radiance Interferometer (AERI) measures the absolute infrared spectral radiance of the sky directly above the instrument (Knuteson et al. 2004). The AERI observes downwelling infrared radiance from 3 to 19 μm at 1 wavenumber resolution, and may enable better retrievals of aerosol optical and physical properties. Our approach uses observations in the 3-4 μm region, where scattering dominates the observed signal during the daytime.

The size distribution of aerosols is critical when studying climatic and human health impacts. Other aerosol retrieval methods generally use wavelengths below 1 μm where they are primarily sensitive to accumulation mode particles, but the AERI's signal will have a significant contribution from the larger aerosols in the size distribution (Figure 1).

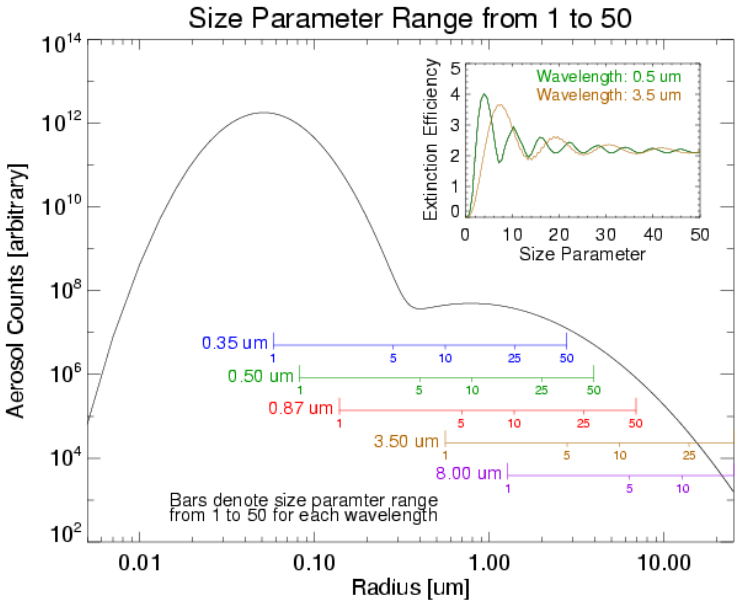

Figure 1. Aerosol sizes distribution and size parameter range.

Methodology

A sensitivity study was performed over a range of bi-modal aerosol size distributions and compositions (ammonium sulfate, ammonium nitrate, and dry dust), where downwelling radiance was computed using the LBLDIS (Turner 2004) model (a combination of the LBLRTM and DISORT radiative transfer models). Atmospheric temperature and gaseous conditions were specified by radiosonde observations. Calculations were made for a range of aerosol density profiles, aerosol compositions, and particle size distributions.

We focused our study on May 10th, 2003 during the ARM Aerosol Intensive Operational Period (IOP) at the Southern Great Plain (SGP) site, a day with an interesting and dynamic aerosol event. Spectral comparisons (obs-calc) were made using assumed aerosol loadings to determine whether the aerosol signal was strong enough to overcome instrument noise constraints and uncertainties in the observed water vapor, and to determine whether the spectral signature could reveal the aerosol composition.

MIXCRA, a mixed-phase cloud property retrieval algorithm (Turner 2004), was modified to retrieve AOD from the AERI observations. The method requires that the size distribution and refractive indices of the scatterers be specified. MIXCRA was run three times, where each run assumed a different number of giant mode aerosols relative to the number of accumulation mode aerosols. MFRSR-derived AODs at 500 nm were used together with the MIXCRA retrievals to infer the relative number of giant mode aerosols.

Aerosol Description

Composition

The composition of atmospheric aerosols is very diverse. For this study, we assumed the aerosols were composed of ammonium sulfate, ammonium nitrate, or dust. The refractive indices of the first two were provided by A.A. Lacis (Lacis), while the refractive indices of the dust were compiled by E.P. Shettle (Shettle and Fenn 1979). All aerosols were assumed to be spherical.

Size Distribution

Bi-modal lognormal size distributions with radius peaks at 0.06 and 1.4 μm, and widths of 0.4 and 0.76 μm respectively, were generated. The smaller particles are characteristic of accumulation mode aerosols, and the larger sizes represent the giant mode particles. The ratio of the number of total accumulation mode particles to the giant mode particles was varied between two (X2) to five (X5) orders of magnitude. Figure 1 shows the X3 size distribution. The size parameter range is shown to indicate which wavelengths are sensitive to Mie scattering. The AERI spectra (brown and purple lines) do not overlap with the accumulation mode and therefore are not sensitive to the smaller aerosols. But the ultraviolet, visible, and near-infrared (IR) channels (blue, green, and red lines, respectively) are very sensitive to the accumulation mode particles.

Sensitivity Study

Scattering in the Infrared

For the atmospheric profile on May 10th, the 3-4 μm region had a much stronger scattering signal than the 10 μm region of the AERI spectrum (Figure 2), about 30% compared to 4%.

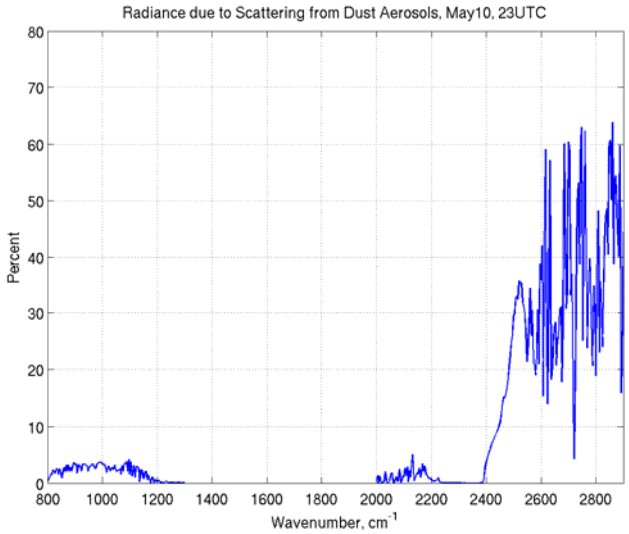

Figure 2. Fraction of daytime signal from scattering as a function of wavenumber.

Uncertainty and Signal Analysis

A "noise spectrum" was calculated as a sum of instrumentation and water vapor uncertainties, assuming a 5% uncertainty in water vapor. Figures 3 and 4 show that the noise is dominated by the water vapor uncertainty in the 10 μm region and by instrument uncertainty in the 3-4 μm region on May 10th. The values change with atmospheric profiles, but the magnitudes were fairly constant for the SGP conditions seen during the IOP.

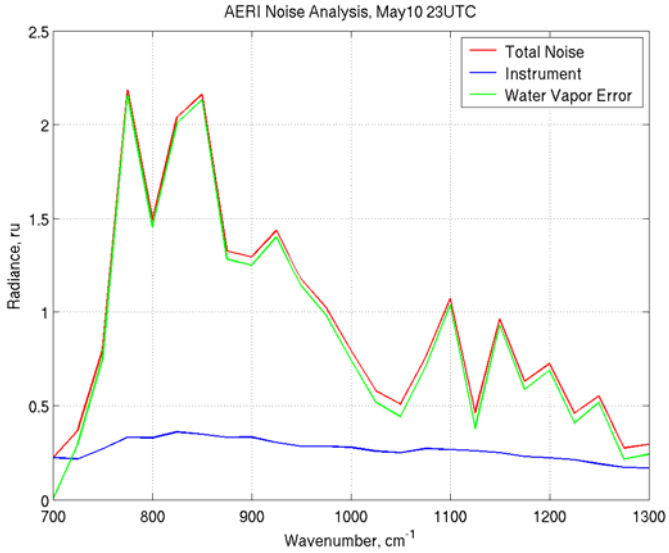

Figure 3. The "noise" in the longer wavelength region of AERI is taken to be the sum of instrument noise and water vapor uncertainty.

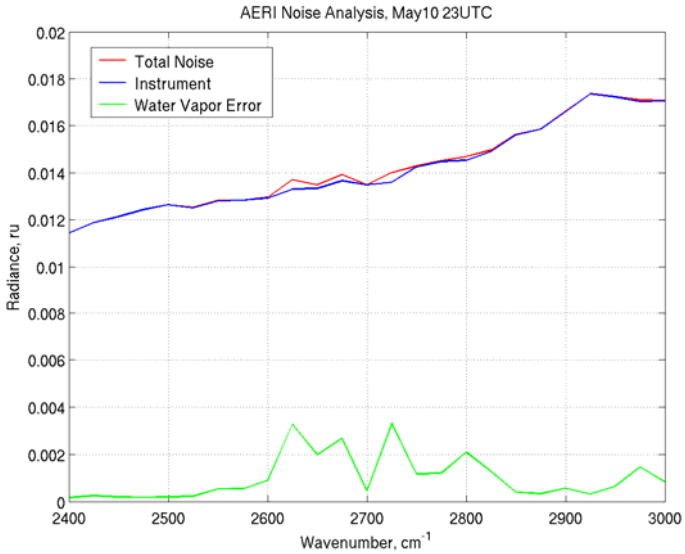

Figure 4. The same as Figure 3, except for the shorter wavelength region of AERI.

Figures 5 and 6 are the best fits to the AERI spectra on May 10th at 13 utc for the X3 size distribution. The 10 μm region's aerosol signal (the difference with clear sky radiances) is weak and has the same magnitude as a 5% uncertainty in water vapor. In contrast, the aerosol signal in the 3-4 μm region for the three aerosol types is above the noise. These vary with atmospheric conditions, but the examples given are representative.

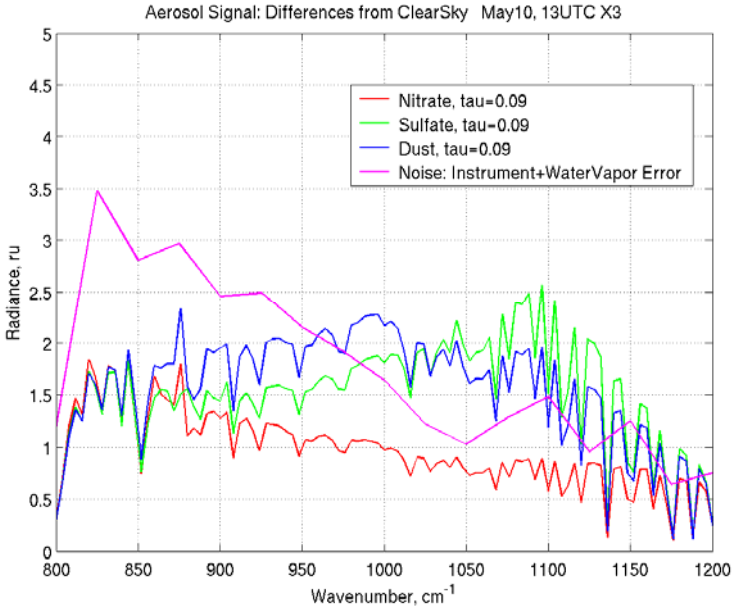

Figure 5. Aerosol signal (difference from clear sky) in the longer wavelength region of AERI.

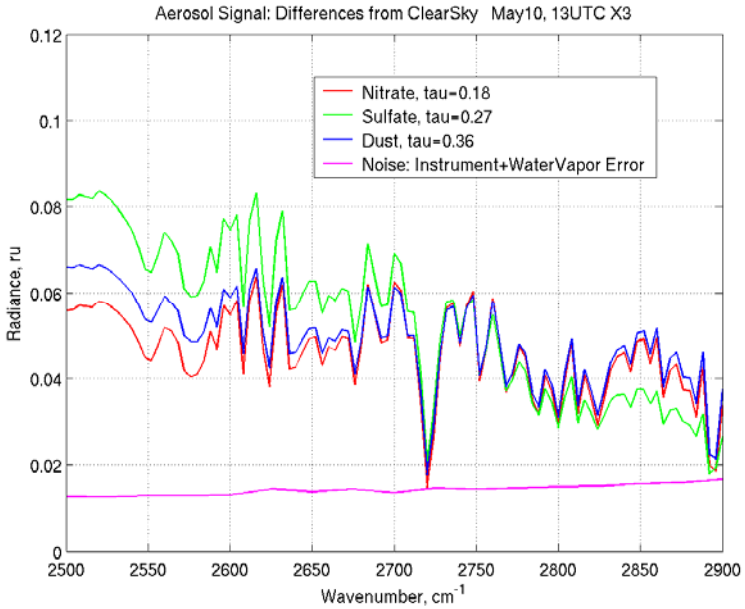

Figure 6. Aerosol signal (difference from clear sky) in the shorter wavelength region of AERI.

Observations

The Raman lidar (RL) provided vertical profiles of water vapor mixing ratio and the aerosol extinction for May 10 (Figures 7 and 8). From 12 utc up to nearly 15 utc we see a significant aerosol layer near the surface; this period has the highest AOD during the IOP. A frontal boundary moved through the region near 16 utc, modifying the aerosol conditions dramatically. Optically thin clouds can be seen at 17 utc at 4 km and at 2 km from 21-22 utc.

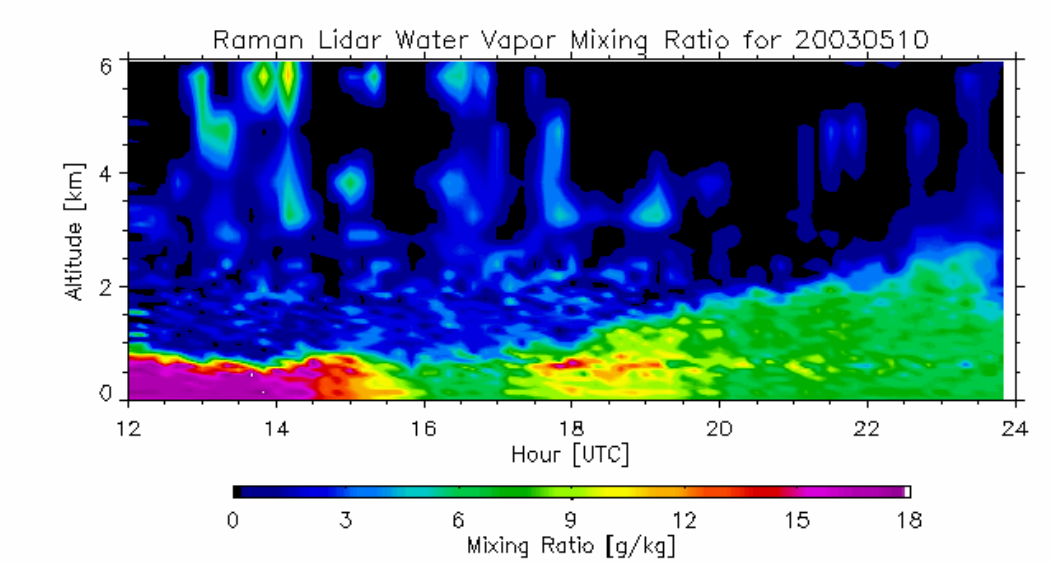

Figure 7. Raman lidar water vapor mixing ratio profiles. The elevated humidity layer correlates well with the aerosol layer in Figure 8.

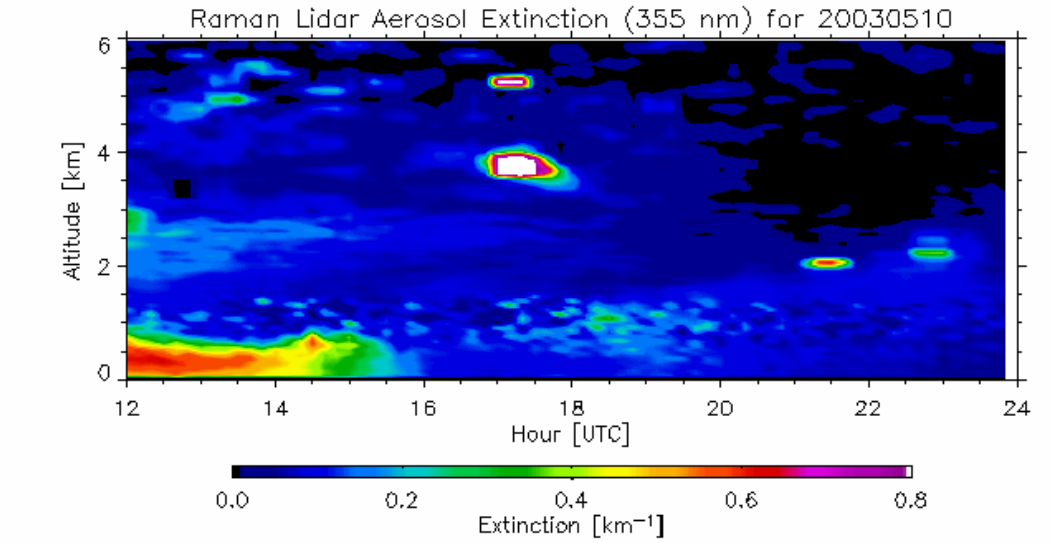

Figure 8. Raman lidar aerosol extinction profiles. There is a significant aerosol layer near the surface from 12 to 15 utc; however, the aerosol loading is significantly smaller after the front passed over the site around 16 utc. Clouds are evident at 17 utc at 4 km and 2 km, 21-23 utc.

Clouds and water vapor uncertainty are large problems in aerosol detection from the AERI. Figure 9a shows the PWV initially used in MIXCRA with the corresponding results in Figure 9b. Using the microwave radiometer (MWR)-derived PWV in MIXCRA (run 2 in Figure 9b) had a large impact on the MIXCRA retrievals, especially from 12-16 utc.

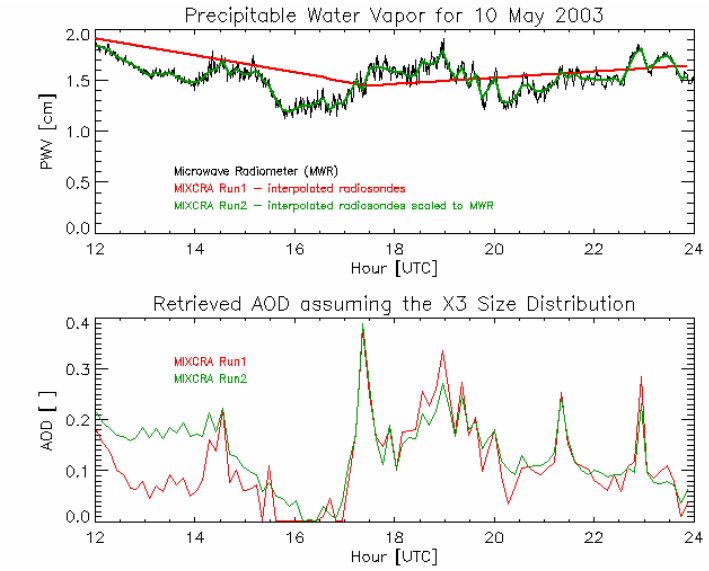

Figure 9a. Perceptible water vapor from interpolated sonde values (red) and scaled to the microwave radiometer (green) used in MIXCRA. The MWR observations are given in black. **Figure 9b**: MIXCRA retrieved AOD using both water vapor assumptions.

Aerosol Optical Depth Retrievals

Aerosol optical depths were retrieved with MIXCRA, assuming a dust composition and the X3 size distribution (Figure 9b). The retrieved AOD, ranging from 0 to 0.4, failed during the frontal passage (15 to 17 utc), and produced anomalous spikes that correspond with clouds (at 17, 21 and 23 utc). The water vapor adjustment made the most difference in the early morning, 12 to 14 utc, when the radiosonde did not capture the rapidly varying structure of the atmosphere. As expected, the retrieval method fails in cloudy conditions when its signal is wrongly attributed to aerosols.

The Normal Incidence Multi-Filter Radiometer (NIMFR) measures the shortwave spectral direct normal irradiance, and is used to infer clear sky AOD at 500 nm (Figure 10, black stars). The MIXCRA retrieved aerosol optical depths for dust and size distributions X2, X3, and X4 are also plotted (red, green, blue lines, respectively). The MIXCRA retrievals are extremely sensitive to the relative number of giant mode aerosols. Therefore, the NIMFR AOD data can be used together with the suite of MIXCRA runs to estimate the relative number of giant mode aerosols. Figure 11 shows the relative number of accumulation mode aerosols (in terms of orders of magnitude) to the number of giant mode aerosols that was determined from the NIMFR – MIXCRA results. From 12 to 14 utc, the NIMFR – MIXCRA results suggest that there are approximately 3.5 orders of magnitude more accumulation mode particles than giant mode particles, whereas after 18 utc there is only an approximately 3.2 orders of magnitude difference between the number of accumulation and giant mode aerosols.

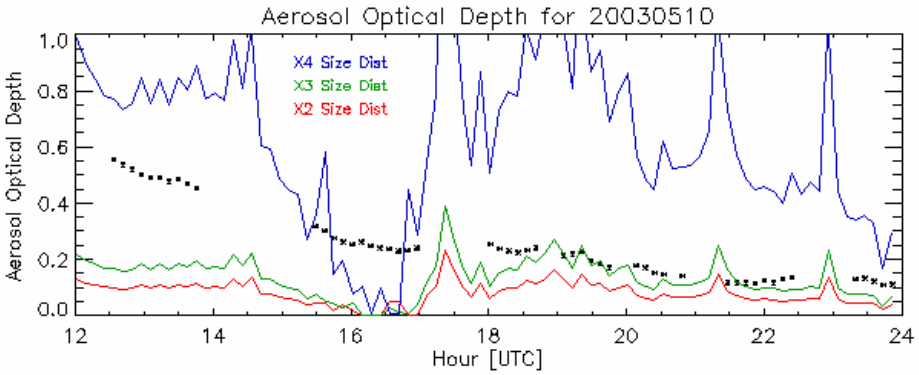

Figure 10. MINFR (black stars) and MIXCRA retrieved aerosol optical depths for X2, X3, and X4 aerosol size distributions (red, green, blue lines).

The aerosol observing system (AOS) is the primary platform for in situ aerosol measurements at the surface. Unfortunately, its passive cavity aerosol spectrometer probe, which makes size-resolved observations of aerosol concentrations, was out-of-order on this day. We have looked at the difference of the total scattering observed by the nephalometer for the 10 μm and 1 μm size cuts as a surrogate for the supermicron scattering. This difference (Figure 11) suggests that, at the surface, there is a larger contribution from supermicron particles from 12-15 utc than from times after 16 utc. However, the NIMFR − MIXCRA results suggest there are relatively fewer large aerosols early in the day relative to later in the day. We do not understand this apparent contradiction, but think it may be due to a difference in where the measurements were made (surface in situ vs. column-averaged measurements). Also, our retrieval may be biased by water vapor uncertainties.

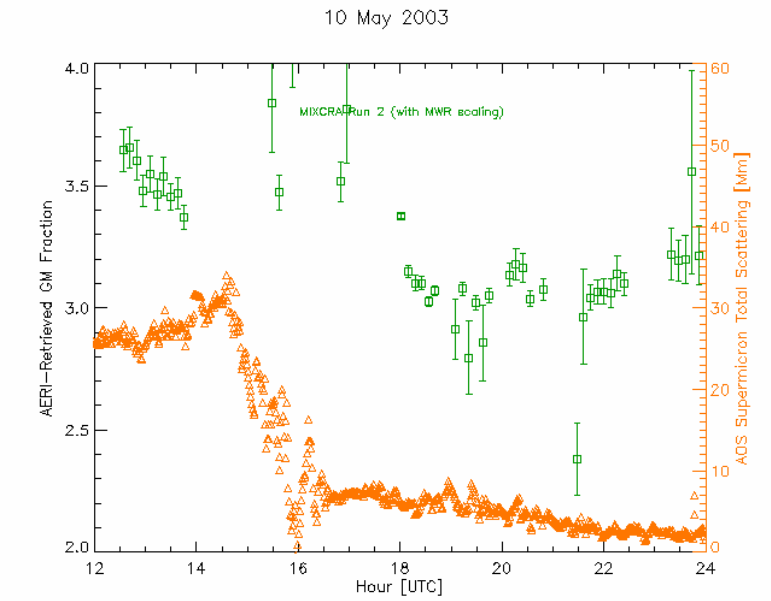

Figure 11. Relative number of accumulation mode aerosol particles to giant mode particles retrieved from NIMFR and AERI data using the MWR-scaled water vapor (squares). The AOS supermicron scattering is the difference of the total scattering measured by the nephalometer at 500 nm with the 10 μm size cut relative to the 1 μm size cut (triangles).

Spectral Signature of Aerosol Composition

The spectral variation in the refractive indices of different aerosol compositions may allow for the determination of composition from AERI observations. For data collected on 10 May 2003 at 13 utc, the optical depths were chosen for three different aerosol types so they would produce the same radiance values as AERI observations at 2550 cm^{-1} (Figure 12).

The AERI observed aerosol signal is shown in black. The aerosol signal for the three compositions show unique spectral characteristics away from 2550 cm^{-1}; the lines diverge for the different aerosol compositions (red, green, blue lines). Specifically consider the two regions near 2650 and 2825 cm^{-1}. In the first region, the dust and sulfate track closely to the AERI observation while the nitrate diverges. And in the second region the nitrates and dust are closer to the AERI observations than the sulfate. Overall, the dust is the aerosol composition which best match the AERI observations.

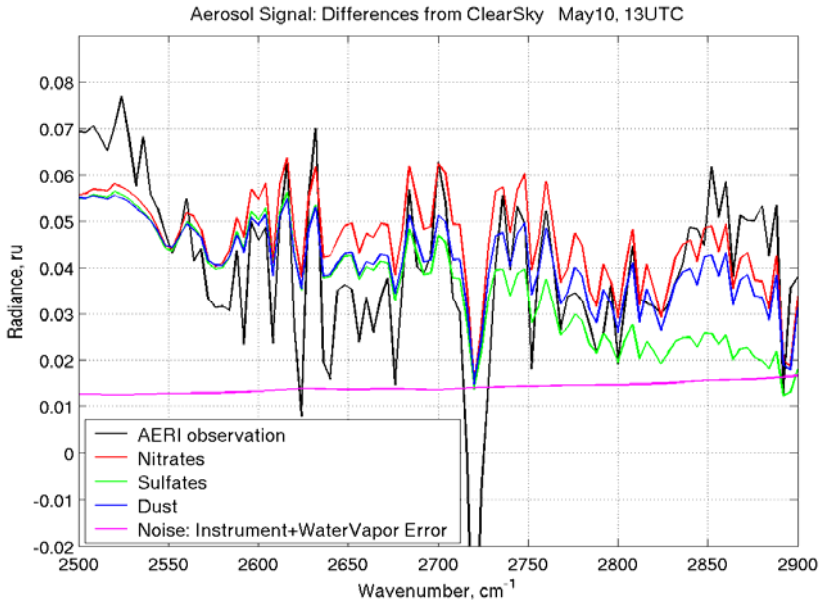

Figure 12. Spectral signatures from ammonium nitrate, ammonium sulfate, and dry dust aerosol.

Conclusions

Theoretical study suggests AERI's IR aerosol signal is strong enough to overcome instrument noise constraints and uncertainties in the water vapor, especially in the 3-4 μm band. The IR aerosol signal dominated by the larger aerosols in the size distribution, unlike other aerosol retrieval methods. In clear sky conditions, the MIXCRA algorithm is able to retrieve AOD for an assumed size distribution and composition, and when used with visible AOD (such as from the NIMFR), can infer the ratio of giant to accumulation mode particles. Different aerosol compositions have unique spectral signatures which can be exploited for retrievals.

Acknowledgement

We would like to thank Andy Lacis for providing us with the refractive indices for ammonium nitrate and ammonium sulfate, and Rich Ferrare for help in understanding the overall picture of the site conditions and data sets available during the Aerosol IOP.

We gratefully acknowledge the Department of Energy support through Grant DE-FG02-90ER61057.

Point of Contact

Corresponding author address Leslie Moy, Cooperative Institute for Meteorological Satellite Studies, University of Wisconsin-Madison, 1225 West Dayton Street, Madison, WI 53706; E-mail: lesliem@ssec.wisc.edu

References

IPCC 2001: Climate Change. 2001. The Scientific Basis. Contribution of Working Group I to the Third Assessment Report of the Intergovernmental Panel on Climate Change. Cambridge University Press, Cambridge, United Kingdom and New York, NY, USA, 881pp. (Houghton, J.T., Y.Ding, D.J. Griggs, M. Noguer, P.J. van der Linden, X. Dai, K. Maskell, and C.A. Jahnson [eds.])

Knuteson, RO, HE Revercomb, FA Best, NC Ciganovich, RG Dedecker, TP Kirkx, SC Ellington, WF Feltz, RK Garcia, HB Howell, WL Smith, JF Short, and DC Tobin. 2004. "Atmospheric emitted radiance interferometer. Part II: Instrument performance." *Journal of Atmospheric and Oceanic Technology* 21, 1777.

Turner, DD. 2004. "Arctic mixed-phase cloud properties from AERI-lidar observations: Algorithm and results from SHEBA." *Journal of Applied Meteorology*, in press.

Lacis, AA, personal communication.

Shettel, EP, and RW Fenn. 1979. "Models for the aerosols of the lower atmosphere and the effects of humidity variations on their optical properties." AFGL-TR-79-0214, Environmental Research Paper No. 675, NTIS, ADA 085851, 94 pp.